NOMA Transmission for Active STAR-RIS Aided Near-Field Communications

Sutanu Ghosh*, Keshav Singh*, Cunhua Pan†, Chih-Peng Li*, and Zhiguo Ding‡
*Institute of Communications Engineering, National Sun Yat-sen University, Kaohsiung 80424, Taiwan
§School of Information Science and Engineering, Southeast University, Nanjing 210096, China
‡School of Electrical and Electronic Engineering, The University of Manchester, Manchester, UK
‡Department of Electrical Engineering and Computer Science, Khalifa University, Abu Dhabi, United Arab Emirates
Email: sutanu99@gmail.com, keshav.singh@mail.nsysu.edu.tw, cpan@seu.edu.cn,
cpli@faculty.nsysu.edu.tw, zhiguo.ding@ku.ac.ae

***Abstract*—To achieve high spectrum efficiency, the utilization of reconfigurable intelligent surface (RIS) may extend the range of near-field region beyond Rayleigh distance. However, an accurate channel model is essential to realize the radiation pattern of near-field communication. This paper studies the performance of an active simultaneous refracting/transmitting and reflecting (STAR)-RIS-aided near-field communication system over Rician fading channels. The transmitter sends information to multiple Internet-of-Things devices (IoDs) through STAR-RIS by applying the non-orthogonal multiple access (NOMA) principle. To better characterize the effect of channel correlation on the performance of the system, a more practical spatial channel correlation model is adapted. In order to show the system performance, the expressions of the outage probability, and the ergodic sum rate of the proposed system are derived and the impacts of the channel estimation errors and imperfect interference cancellation on those performance metrics are depicted through the results. The results reveal the performance degradation through the correlated channel with respect to uncorrelated channels.**

***Index Terms*—Near-field communication, simultaneous refracting/transmitting and reflecting reconfigurable intelligent surface, non-orthogonal multiple access.**

I. INTRODUCTION

To achieve the goal of higher signal coverage with spectrally and energy efficient communications for the next-generation wireless networks, reconfigurable intelligent surface (RIS) has been recognized as a promising technique to improve the system coverage [1]. The signal reflection from RIS is controlled through the intelligent adaptation of the amplitude responses and phase shifts of a large number of active/passive scattering elements. To address the limit of the maximum 180° space coverage of conventional RIS, simultaneous refracting/transmitting and reflecting (STAR)-RIS has been developed to increase the degrees-of-freedom (DoF) [2]. STAR-RIS operates by applying the energy splitting (ES), mode switching (MS), or, time switching (TS) protocols [3]. In addition to that, the limitation of double fading attenuation of passive RIS can be eliminated by using active RIS architecture. As an incident signal is amplified using active RIS, the strength of received signal is increased directly. The performance improvement using active RIS over passive RIS was reported in [4]. Moreover, various system performance metrics were analysed by adapting different channel models in various existing contributions [5], [6], where some of them also considered more practical channel correlation models in STAR-RIS to realize the impact of them on the system performance [7]–[9].

This work was supported in part by the National Science and Technology Council of Taiwan under Grant NSTC 113-2218-E-110-009, Grant NSTC 112-2221-E-110-029-MY3, and in part by the Sixth Generation Communication and Sensing Research Center funded by the Higher Education SPROUT Project, the Ministry of Education of Taiwan.

Since non-orthogonal multiple access (NOMA) [10] is beneficial for ultra-reliability and low-latency communications, several investigations were done to analyse the system performance applying NOMA in STAR-RIS-aided wireless networks to enhance the spectral efficiency [11]. The study of the ergodic capacity, outage probability analysis of STAR-RIS was done in [6] over Rician fading channels. To achieve further enhancement of the spectral efficiency by serving multiple users/devices, the utilization of an extremely large antenna array (ELAA) was proposed in upcoming 6G communication [12]. Due to the sharp enhancement of the antenna aperture in ELAA or the usage of RIS, range of near-field region can be significantly expanded. Recall that boundary limit between the near-field and far-field regions is defined by Rayleigh distance $\left(\frac{2D^2}{\lambda}, D \text{ is array aperture and } \lambda \text{ is the wavelength of the carrier signals}\right)$. As the properties of the far-field channel model are not the same as near-field channels, the concept of the far-field model leads to a mismatch in the practical near-field channel, which potentially results in performance losses in near-field communication. To realize the radiation pattern of both near-field and far-field channels and to distinguish the channel model in form of their properties, different mathematical modeling for two different channels were proposed in [13], [14].

The previous works on RIS-aided networks considered correlated channels and channel hardening issues [7]–[9], [15]. The effect of the expansion of the near-field region was not under their consideration. On the other hand, the existing works [13], [14] on the modelling of near-field communication did not consider the multiple access techniques to support multiple users to enhance spectrum efficiency. Motivated by all these issues, we study the system performance of a power-

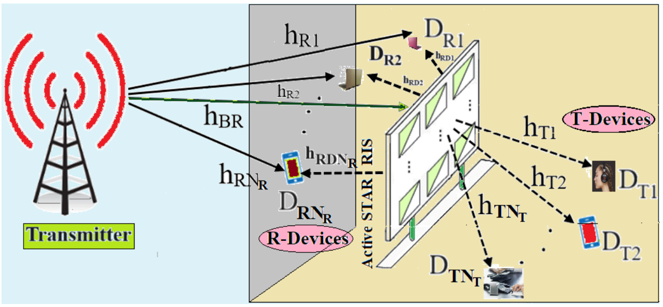

Fig. 1: Active STAR-RIS-aided near-field communication system.

domain NOMA-based communication between a transmitter and multiple Internet-of-Things devices (IoDs) via an STAR-RIS to support specific Internet-of-Things (IoT) services, such as virtual reality, remote control of autonomous vehicles, etc. to achieve higher reliability [16]. The application of the model is considered for the transmission in a conference room, where STAR-RIS is placed in the middle of the room. The contributions of the paper are listed below:

- We adopt a spatial correlation model for the transmission through RIS and use the near-field and far-field channel models to derive the expressions of the signal-to-interference plus noise ratio (SINR), outage probability (OP) and ergodic sum rate. To tackle the double fading attenuation issue, an active STAR-RIS configuration is explored.
- The performance of the considered scheme is analysed for a more realistic imperfect channel state information (ICSI)-imperfect successive interference cancellation (ISIC) environment. The performance comparison between the near-field and far-field channels is also shown.
- Furthermore, Monte-Carlo simulation is executed to verify the accuracy of all the developed analytical expressions, and the impacts of near-field and far-field communication on the system performances are highlighted.

II. System Architecture and Signal Modelling

Description of System Model: As illustrated in Fig. 1, the system model consists of a transmitter, an active STAR-RIS, N_R reflecting IoDs (R-Devices (RDs), $i \in 1, 2, \ldots, N_R$ and denoted as D_{Ri}) and N_T transmitting/refracting IoDs (T-Devices (TDs), $i \in 1, 2, \ldots, N_T$ and denoted as D_{Ti}). The transmitter communicates with D_{Ri} over the direct path and through the support of the STAR-RIS. Besides, RIS is equipped with $L_a = L_{ah} \times L_{av}$ elements, where L_{ah} and L_{av} indicate the numbers of configuring elements in horizontal direction and vertical direction, respectively. We assume that transmitter and IoDs are associated with a single antenna. For energy efficient operation, the whole operations are performed in the energy splitting (ES) mode [5]. Reflecting and transmitting matrices are defined as $\mathbf{\Phi}_R$=diag $(\sqrt{\eta_1^r\zeta_1^r}e^{j\phi_1^r}, \sqrt{\eta_2^r\zeta_2^r}e^{j\phi_2^r}, \ldots, \sqrt{\eta_{L_a}^r\zeta_{L_a}^r}e^{j\phi^r_{L_a}})$ and $\mathbf{\Phi}_T$=diag $(\sqrt{\eta_1^t\zeta_1^t}e^{j\phi_1^t}, \sqrt{\eta_1^t\zeta_2^t}e^{j\phi_2^t}, \ldots, \sqrt{\eta_1^t\zeta_{L_a}^t}e^{j\phi^t_{L_a}})$, respectively [17], where ϕ_i^r, ζ_i^r and ϕ_i^t, ζ_i^t are the phase shifts and amplitude coefficients of the i-th element reflecting and transmitting responses, respectively, and specifically, ϕ_i^r, ϕ_i^t $\in [0, 2\pi)$. Moreover, $1 < \eta_i^r, \eta_i^t \leq \eta_{max}$ (η_{max} is the maximum value) are the i-th element reflecting and refracting mode amplification factors [18]. In addition to that, due to the law of energy conservation, we have $\zeta_i^r + \zeta_i^t = 1$ ($\forall i \in N_R, N_T$) [19].

The channel gains between different links transmitter $\rightarrow$ l-th element of STAR-RIS, transmitter $\rightarrow$ D_{Ri}, l-th element of STAR-RIS $\rightarrow$ D_{Ri} and l-th element of STAR-RIS $\rightarrow$ D_{Ti} are h_{Bl}, h_{BRi}, h_{lRi} and $\mathbf{h}_{lTi}$, respectively. All the channels between transmitter–RDs, STAR-RIS–IoDs and transmitter–STAR-RIS follow the independent identically distributed (IID) Rician distribution as follows: $h_\iota = \left(\sqrt{\frac{\kappa}{\kappa+1}}h_\iota^{LoS} + \sqrt{\frac{1}{\kappa+1}}h_\iota^{NLoS}\right)$, where κ indicates Rician factor. Transmitter to STAR-RIS channel vector for RDs and TDs are defined as $\mathbf{h}_{Br} = (h_{B1}, h_{B2}, \ldots, h_{BL_a})^T$, $\mathbf{h}_{Br}^{NLoS} \sim \mathcal{CN}(0, \mathbf{R}_{Br})$ ($r \in 1, 2, \ldots, L_a$) and specifically $h_{BRi}^{NLoS} \sim \mathcal{CN}(0,1)$ for scattered signals. $\mathbf{h}_{r\aleph i} = (h_{1\aleph i}, h_{2\aleph i}, \ldots, h_{L_a\aleph i})^T$ ($\forall \aleph \in R, T$). λ is wavelength, d_ι is antenna spacing and θ_a indicates the angle of arrival. R_ι is the covariance term. The proposed system is considered under the conditions of imperfect channel estimation and ISIC. ν is used to define the propagation path loss constant.

Near-field communication: The transmitter applies power-domain NOMA to send the following information to IoDs. The received signal at D_{Ri} is written as

$$Y_{Ri} = \left(\frac{\sum_{l=1}^{L_a}\hat{h}_{Bl}\sqrt{\alpha_l^r}\hat{h}_{lRi}e^{j\phi_{l,Ri}} + e_{Ri}}{\sqrt{\beta_{Rl}}} + \frac{\hat{h}_{BRi} + e_{Ri}}{\sqrt{\beta_d}}\right) \times \sqrt{P_B}\Big(\sum_{i=1}^{N_R}\sqrt{a_i}X_{ri} + \sum_{i=1}^{N_T}\sqrt{b_i}X_{ti}\Big) + n_{Ri}, \quad (1)$$

where $\alpha_l^r = \eta_l^r \times \zeta_l^r$, ϕ_l^{Bl} and ϕ_l^{lRi} are the phase angle of channel gain between transmitter and l-th RIS element and the phase angle of channel gain between l-th RIS element and D_{Ri}, respectively and $\phi_{l,Ri} = \phi_l^{Bl} + \phi_l^r + \phi_l^{lRi}$. $\hat{h}_{Bl}$ is the estimated channel gain between transmitter and l-th element of RIS and $\hat{h}_{lRi}$ is the estimated channel gain between l-th element of RIS and i-th RD. n_{Ri} and e_{Ri} $\sim$ $\mathcal{CN}(0, \sigma_R^2)$ indicate noise and channel estimation error at D_{Ri}, respectively. P_b is the transmission power of transmitter. Without loss of generality, the distances are considered to be ordered as follows $d_{lg1} \leq d_{lg2} \leq \cdots \leq d_{lgN_g}$, ($\forall g \in R, T$) and thus, the power coefficients are allocated as follows $0 < \Delta_1 P_B \leq \Delta_2 P_B \leq \cdots \leq \Delta_{N_g}P_B < 1$. $\Delta_i \in a_i, b_i$ are the power coefficients to transmit the messages for RDs and TDs, respectively and $\sum_{i=1}^{N_R}a_i + \sum_{i=1}^{N_T}b_i = 1$. X_{ri} and X_{ti} are the signals for D_{Ri} and D_{Ti}. Similar to (1), the received signal at D_{Ti} is expressed as

$$Y_{Ti} = \left(\frac{\sum_{l=1}^{L_a}\hat{h}_{Bl}\sqrt{\alpha_l^t}\hat{h}_{lTi}e^{j\phi_{l,Ti}} + e_{Ti}}{\sqrt{\beta_{Tl}}}\right) \times\sqrt{P_B}\Big(\sum\nolimits_{i=1}^{N_R}\sqrt{a_i}X_{ri} + \sum\nolimits_{i=1}^{N_T}\sqrt{b_i}X_{ti}\Big) + n_{Ti}. \quad (2)$$

Here, $\alpha_l^t = \eta_l^t \times \zeta_l^t$, ϕ_l^{lRi} is the phase angle of channel gain between l-th RIS element and D_{Ti} and $\phi_{l,Ti} = \phi_l^{Bl} + \phi_l^t + \phi_l^{lTi}$. $\hat{h}_{lTi}$ is the estimated channel gain between l-th element of RIS and i-th TD. n_{Ti} and $e_{Ti} \sim \mathcal{CN}(0, \sigma_T^2)$ indicate noise and channel estimation error at D_{Ti}, respectively. The path loss component of the direct link is $\beta_d \triangleq \frac{64\pi^3 d_i^\nu}{\lambda^2 G_T G_R G d_x d_y |\gamma_a^2|}$. End-to-end channel path loss via l-th element is $\beta_{gl} \triangleq \frac{(4\pi)^3 (d_{bl} d_{lgi})^\nu}{\lambda^2 G_T G_R G d_x d_y |\gamma_g^2| F_{gi}^{\text{combine}}}$. The diension of each unit RIS cell is defined by the width d_x and the length d_y. The joint normalized power radiation pattern $F_{gi}^{\text{combine}} \triangleq (\cos\theta_{gl}^{bx})^{\frac{G_t}{2}-1} \cos(\theta_{gl}^b)\cos(\theta_{gl}^i)(\cos\theta_{gl}^{ix})^{\frac{G_r}{2}-1}$, $\cos\theta_{gl}^{bx} = \frac{d_{BR}^\nu + (d_{bl})^\nu - d_l^\nu}{2 d_{BR} d_{bl}}$, $\cos\theta_{gl}^{ix} = \frac{d_{gi}^\nu + (d_{lgi})^\nu - d_l^\nu}{2 d_{Ri} d_{lgi}}$, $\cos\theta_{gl}^b = \frac{z_b - z_0}{d_{bl}}$, $\cos\theta_{gl}^i = \frac{z_b - z_0}{d_{lgi}}$ [13]. d_{bl} is the distance between transmitter and l-th element of the RIS, d_{lgi} is the distance between l-th element of the RIS and D_{gi}. θ_{gl}^{bx} and θ_{gl}^{ix} are the elevation angles from transmitter antenna and i-th g-device antenna to l-th reflecting element of RIS, respectively.

While, θ_{gl}^b and θ_{gl}^i are the elevation angles from the l-th reflecting element of RIS to transmitter antenna and i-th g-device antenna, respectively. d_{BR}, d_{gi}, d_i and d_l indicate the distances between the transmitter and the center of RIS, distance between D_{gi} and the center of RIS, distance between D_{gi} and transmitter and distance between l-th element of RIS and the center of RIS. $|\gamma_g^2|$ and $|\gamma_a^2|$ are the ratios of the output signal to the incident signal, $e_{gi} \sim \mathcal{CN}(0, \sigma_g^2)$ and n_{gi} are channel estimation errors due to ICSI at D_{gi} and additive white Gaussian noise (AWGN) at D_{gi}, respectively. Centralized deployment is considered for all the nodes present in the system and centralized location of transmitter, STAR-RIS and D_{gi} are (x_b, y_b, z_b), (x_0, y_0, z_0) and (x_{gi}, y_{gi}, z_{gi}), respectively.

Far-field communication: The path loss model of (1) and (2) can be simplified further for far-field communication following $d_l << d_{bl} \approx d_{BR}$ and $d_l << d_{lgi} \approx d_{gi}$. Consequently, $\cos\theta_{gl}^{bx}$ and $\cos\theta_{gl}^{ix}$ are approximated as 1.

$$\beta_{gl}^{\text{far field}} \triangleq \frac{(4\pi)^3 (d_{BR} d_{gi})^\nu}{\lambda^2 G_T G_R G d_x d_y \mid \gamma_g^2 \mid \cos(\theta_{gl}^b)\cos(\theta_{gl}^i)}. \quad (3)$$

Following correlation model in [15], each element of R_ι must satisfy

$$[R_\iota]_{m,n} = \frac{sin\left(\frac{2\pi}{\lambda} \mid\mid a_m - a_n \mid\mid\right)}{\frac{2\pi}{\lambda} \mid\mid a_m - a_n \mid\mid}, \quad m, n \in \{1, ..., N_\iota\}. \quad (4)$$

where $a_m = \left[0, mod(m-1, N_{\iota h}) d_{\iota h}, \left\lfloor \frac{m-1}{N_{\iota h}} \right\rfloor d_{\iota v}\right]^T$.

SNR Characteristics: As RDs and the transmitter are located at the same side, successive interference cancellation (SIC) is applied to first detect and then remove the signals of TDs signals. Consequently, RDs are able to decode their own signals. Therefore, the SINR for RDs to decode the signals of TDs can be written as

$$\Upsilon_{Ri \to Ti} = \frac{A_{p1}^2 \frac{\sum_{i=1}^{N_T} b_i P_B}{\sigma^2}}{A_{p1}^2 \frac{\sum_{i=1}^{N_R} a_i P_B}{\sigma^2} + \sigma_R^2 \left(\frac{1}{\beta_{Rl}} + \frac{1}{\beta_d}\right) \frac{P_B}{\sigma^2} + 1}, \quad (5)$$

where σ^2 is used to define AWGN noise variance. After applying SIC, the SINR output at D_{Ri} is expressed as

$$\Upsilon_{Ri} = \frac{A_{p1}^2 \frac{a_i}{\sigma^2}}{\frac{A_{p1}^2 \sum_{t_s=1, t_s \neq i}^{N_R} a_{t_s}}{\sigma^2} + \frac{A_{p1}^2 \varkappa_i}{\sigma^2} + \frac{\sigma_R^2}{\beta_{Rl}\sigma^2} + \frac{\sigma_R^2}{\beta_d \sigma^2} + \frac{1}{P_B}}, \quad (6)$$

where $\varkappa_i (\in [0, 1])$ is the SIC imperfection error due to the reason of ISIC of TDs at D_{Ri}. The SINR output at D_{Ti} to decode its own signal by treating the signal of RDs as the interference can be written as

$$\Upsilon_{Ti} = \frac{A_{p2}^2 \frac{b_i}{\sigma^2}}{\frac{A_{p2}^2 \sum_{t_w=1, t_w \neq i}^{N_T} b_{t_w}}{\sigma^2} + \frac{A_{p2}^2 \sum_{i=1}^{N_R} a_i}{\sigma^2} + \frac{\sigma_T^2}{\beta_{Tl}\sigma^2} + \frac{1}{P_B}}, \quad (7)$$

where $A_{p1} = \left(\frac{|\hat{h}_{BRi}|}{\sqrt{\beta_d}} + \sum_{l=1}^{L_a} \frac{\sqrt{\alpha_l^r} e^{j\phi_{l,Ri}} |\hat{h}_{Bl} \hat{h}_{lRi}|}{\sqrt{\beta_{Rl}}}\right)$ and $A_{p2} = \left(\sum_{l=1}^{L_a} \frac{\sqrt{\alpha_l^t} e^{j\phi_{l,Ti}} |\hat{h}_{Bl} \hat{h}_{lTi}|}{\sqrt{\beta_{Tl}}}\right)$.

Channel Model: As the various channels h_{BR}, h_{RDil}, h_{Ril} and h_{Til} follow Rician distribution, the probability density function (PDF) of those channels can be expressed as

$$f_h(u) = \frac{2u(\kappa+1)e^{-u^2(\kappa+1)}}{e^{(\kappa)}} I_0(2u\sqrt{\kappa(\kappa+1)}), \ u > 0, \quad (8)$$

where $I_0(.)$ indicates modified Bessel function of first kind with 0-th order. $Q_{\mathscr{M}}(.,.)$ is Marcum Q-function with order $\mathscr{M}$. Rician factor $\kappa = \frac{A^2}{2\delta^2}$, where A^2 and $2\delta^2$ define the line of sight (LoS) and non-LoS (NLoS) power components, respectively. As $\hat{h}_{Bl}$ and $\hat{h}_{lRi}$ are independent of each other, the PDF of $|\hat{h}_{Bl}||\hat{h}_{lRi}|$ is described as $|\hat{h}_{RD_il}|$. The mean of these variables can be defined as $\mu_{\{|\hat{h}_{Bl}|\}} = \mu_{\{|\hat{h}_{lRi}|\}} = \sqrt{\frac{\pi}{4(\kappa+1)}} L_{\frac{1}{2}}(-\kappa)$, and Laguerre polynomial $L_{1/2}(x) = e^{x/2}\left[(1-x)I_0\left(-\frac{x}{2}\right) - xI_1\left(-\frac{x}{2}\right)\right]$. Then $\mu_{\{|\hat{h}_{Bl}||\hat{h}_{lRi}|\}} = \left(\sqrt{\frac{\pi}{4(\kappa+1)}} L_{\frac{1}{2}}(-\kappa)\right)^2$.

It is considered that $\sum_{l=1}^{L_a}\{|\hat{h}_{Bl}||\hat{h}_{lRi}|\} = |\hat{h}_{R_il}|$ and it is possible to approximate $|\hat{h}_{R_il}|$ by using the central limit theorem. $\hat{h}_{R_il} \sim \mathcal{CN}(\mu_{h_{R_il}}, \sigma_{h_{R_il}}^2)$ and $\mathrm{Var}[\hat{h}_{R_il}] = \mathbb{E}[(\hat{h}_{R_il} - \mathbb{E}[\hat{h}_{R_il}])^2] = \sum_{m=0}^{L_a}\sum_{n=0}^{L_a}\left([\bar{R}_{R_il}]_{m,n}\right)^2 - \frac{\pi^2\left(L_{\frac{1}{2}}(-\kappa)\right)^4}{16(\kappa+1)^2} L_a^2$, where $\bar{R}_{\iota R} \triangleq \mathbb{E}[|h_\iota||h_\iota|^T] = \mathbb{E}[|g_\iota||g_\iota|^T]$ [9]. For, $m \neq n$, $[\bar{R}_{R_il}]_{m,n} = \frac{|[R_{R_il}]_{m,n}|^2 - 1}{2} K\left(|[R_{R_il}]_{m,n}|^2\right) + E\left(|[R_{R_il}]_{m,n}|^2\right)$. For, $m = n$, $[\bar{R}_{R_il}]_{m,n} = 1$. $K(.)$ and $E(.)$ are used to define the complete elliptic integrals of first and second kinds, respectively and mean $\mu_{\hat{h}_{R_il}} = L_a \mu_{\{|\hat{h}_{Bl}||\hat{h}_{lRi}|\}}$. Since $\frac{A}{\delta}$ increases, the Rician distribution becomes more symmetric with the Gaussian distribution [20], therefore, $\hat{h}_{BRi}$ can be approximated as the Gaussian form. Finally, $\left(\frac{|\hat{h}_{BRi}|}{\sqrt{\beta_d}} + \sum_{l=1}^{L_a} \frac{\sqrt{\alpha_l^r} e^{j\phi_{l,Ri}} |\hat{h}_{Bl}\hat{h}_{lRi}|}{\sqrt{\beta_{Rl}}}\right)$ is approximated in form of the Gaussian as $U_{h_{Ri}} = \left(\frac{|\hat{h}_{BRi}|}{\sqrt{\beta_d}} + \sum_{l=1}^{L_a} \frac{\sqrt{\alpha_l^r} e^{j\phi_{l,Ri}} |\hat{h}_{Bl}\hat{h}_{lRi}|}{\sqrt{\beta_{Rl}}}\right)$, $U_{h_{Ri}} \sim \mathcal{CN}(\mu_{u_{h_{Ri}}}, \sigma_{u_{h_{Ri}}}^2)$ and $A_{p1}^2 = U_{h_{Ri}}^2$. The PDF of A_{p1} is approximated by applying the Gamma distribution.

Similarly, we can also approximate $\left[\sum_{l=1}^{L_a} \frac{\sqrt{\alpha_l^t} e^{j\phi_{l,Ti}} |\hat{h}_{Bl}\hat{h}_{lTi}|}{\sqrt{\beta_{tl}}}\right]$ as $U_{h_{Ti}}$ and $U_{h_{Ti}} \sim \mathcal{CN}(\mu_{u_{h_{Ti}}}, \sigma^2_{u_{h_{Ti}}})$, where mean $\mu_{\{|\hat{h}_{lTi}|\}} = \sqrt{\frac{\pi}{4(\kappa+1)}} L_{\frac{1}{2}}(-\kappa)$, $\mu_{\{|\hat{h}_{Bl}||\hat{h}_{lTi}|\}} = \left(\sqrt{\frac{\pi}{4(\kappa+1)}} L_{\frac{1}{2}}(-\kappa)\right)^2$. Moreover, it is considered that $\sum_{l=1}^{L_a}\{| \hat{h}_{Bl} || \hat{h}_{lTi} |\} =| \hat{h}_{T_il} |$ and $\text{Var}[\hat{h}_{T_il}] = \mathbb{E}[(\hat{h}_{T_il} - \mathbb{E}[\hat{h}_{T_il}])^2] = \sum_{m=0}^{L_a}\sum_{n=0}^{L_a}\left([\bar{R}_{T_il}]_{m,n}\right)^2 - \frac{\pi^2\left(L_{\frac{1}{2}}(-\kappa)\right)^4}{16(\kappa+1)^2} L_a^2$. For, $m \neq n$, $[\bar{R}_{T_il}]_{m,n} = \frac{|[R_{T_il}]_{m,n}|^2-1}{2} K(| [R_{T_il}]_{m,n} |^2) + E(| [R_{T_il}]_{m,n} |^2)$. For, $m = n$, $[\bar{R}_{T_il}]_{m,n} = 1$. The PDF of $A_{p2}^2 = U^2_{h_{Ti}}$ can be approximated as same way like A_{p1}.

III. Performance Analysis

Outage Probability Analysis: The end-to-end OPs at both D_{Ri} and D_{Ti} are described as the complement of the successful communication over all the different links. OPs at both D_{Ri} and D_{Ti} are expressed as

$$\mathcal{P}_{Out,Ri} = 1 - \left(\mathscr{P}(\Upsilon_{Ri\to Ti} \geq \Upsilon_R^{th}) \times \mathscr{P}(\Upsilon_{Ri} \geq \Upsilon_R^{th})\right), \quad (9)$$

$$\mathcal{P}_{Out,Ti} = 1 - \mathscr{P}(\Upsilon_{Ti} \geq \Upsilon_T^{th}), \quad (10)$$

respectively, where Υ_R^{th} and Υ_T^{th} are the target signal-to-noise ratio (SNR). The term $\mathscr{P}(\Upsilon_{Ri\to Ti} \geq \Upsilon_R^{th})$ is defined as [21]

$$\mathscr{P}(\Upsilon_{Ri\to Ti} \geq \Upsilon_R^{th}) = \mathscr{P}\left(A_{p1}^2 \geq gp_2\right) = F_{A^2_{p1}}(gp_2), \quad (11)$$

where $F(.)$ is the cumulative distribution function (CDF), $gp_2 = \frac{\Upsilon_R^{th}\left(1+\sigma_R^2\left(\frac{1}{\beta_{Rl}}+\frac{1}{\beta_d}\right)\frac{P_B}{\sigma^2}\right)}{\left(\frac{\sum_{i=1}^{N_T} b_i P_B}{\sigma^2} - \Upsilon_R^{th}\frac{\sum_{i=1}^{N_R} a_i P_B}{\sigma^2}\right)}$, $\Lambda_R = \frac{\mu^2_{u_{hs}}}{\sigma^2_{u_{hs}}} - 1$, $\Omega_R = \frac{\sigma^2_{u_{hs}}}{\mu_{u_{hs}}}$, $\Gamma(.,.)$ indicates upper incomplete gamma function and $\Gamma(.)$ indicates gamma function. Now, $\mathscr{P}(\Upsilon_{gi} \geq \Upsilon_R^{th}) = \mathscr{P}\left(A_{p1}^2 \geq gp_g\right)$, $(\forall gi \in Ri, Ti)$ is expressed as

$$\mathscr{P}(\Upsilon_{gi} \geq \Upsilon_g^{th}) = F_{A^2_{p1}}(gp_g), \quad (12)$$

where $gp_R = \frac{\Upsilon_R^{th}\left(1+\sigma_R^2\left(\frac{1}{\beta_{Rl}}+\frac{1}{\beta_d}\right)\frac{P_B}{\sigma^2}\right)}{\left(\frac{a_i P_B}{\sigma^2} - \Upsilon_R^{th}\left[\frac{\varkappa_i P_B}{\sigma^2} + \frac{\sum_{t_s=1,t_s\neq i}^{N_R} a_{t_s} P_B}{\sigma^2}\right]\right)}$, $gp_T = \frac{\Upsilon_T^{th}\left(1+\sigma_T^2\left(\frac{1}{\beta_{Tl}}\right)\frac{P_B}{\sigma^2}\right)}{\frac{b_i P_B}{\sigma^2} - \Upsilon_T^{th}\left[\frac{\sum_{i=1}^{N_R} a_i P_B}{\sigma^2} + \frac{\sum_{t_w=1,t_w\neq i}^{N_T} b_{t_w} P_B}{\sigma^2}\right]}$, $\Omega_T = \frac{\sigma^2_{u_{ht}}}{\mu_{u_{ht}}}$, $\Lambda_T = \frac{\mu^2_{u_{ht}}}{\sigma^2_{u_{ht}}} - 1$. Based on (11)-(12), the closed form expressions of (9) and (10) can be determined.

Ergodic Sum Rate Analysis: The instantaneous data rate of decoding the message at D_{gi} $(g \in R, T)$ can be expressed as

$$\mathcal{R}_{gi} = \log_2(1 + \Upsilon_{gi}), \quad g \in R, T. \quad (13)$$

On the basis of (13), the ergodic sum rate at D_{gi} is

$$\varepsilon_{gi} = \mathbb{E}[\mathcal{R}_{gi}]. \quad (14)$$

TABLE I: Parameter settings.

Parameter	Value	Parameter	Value	Parameter	Value
ν	2	d_{BR}	15 m [8]	σ^2	-70 dBm
κ	0.8 dB	λ	0.1 m [8]	Υ_T^{th}	-10 dB

Applying the principle of NOMA, the sum rate for RDs/TDs is expressed as

$$\varepsilon_{Sg} = \sum\nolimits_{i\in N} \varepsilon_{gi}. \quad (15)$$

The ergodic sum rate for the information transfer at D_{gi} is

$$\varepsilon_{gi} = \mathbb{E}[\mathcal{R}_{gi}] = \frac{1}{\ln 2}\int_0^\infty \frac{1-\mathcal{F}_{\Upsilon_{gi}}\left(z_i(\epsilon_{gi})\right)}{1+\epsilon} d\epsilon$$
$$= \frac{1}{\ln 2}\int_0^\infty \frac{\frac{\Gamma\left(\Lambda_k+1, \frac{\sqrt{\frac{\epsilon G_{pg}}{C_{pg1}-\epsilon C_{pg2}}}}{\Omega_k}\right)}{\Gamma(\Lambda_k+1)}}{1+\epsilon} d\epsilon = \frac{2\sum_{t_s=0}^{\infty}\sum_{p_a=0}^{\Lambda_k}}{(\ln 2)p_a!}$$
$$\times \frac{(-1)^{t_s}(G_{pg})^{t_u-t_s-1}(C_{pg1})^{t_s+1}\Gamma(p_a+2t_s-2t_u+2)}{\sum_{t_u=0}^{t_s+2}\binom{t_s+2}{t_u}(C_{pg2})^{t_u}(\Omega_k)^{2t_u-2-2t_s}}, \quad (16)$$

where $G_{pR} = 1+\sigma_R^2\left(\frac{1}{\beta_{Rl}}+\frac{1}{\beta_d}\right)\frac{P_B}{\sigma^2}$, $G_{pT} = 1+\sigma_T^2\left(\frac{1}{\beta_{Tl}}\right)\frac{P_B}{\sigma^2}$, $C_{pR1} = \frac{a_i P_B}{\sigma^2}$, $C_{pR2} = \frac{\varkappa_i P_B}{\sigma^2} + \frac{\sum_{t_s=1,t_s\neq i}^{N} a_{t_s} P_B}{\sigma^2}$, $C_{pT1} = \frac{b_i P_B}{\sigma^2}$, $C_{pT2} = \frac{\sum_{i=1}^{N} a_i P_B}{\sigma^2} + \frac{\sum_{t_w=1,t_w\neq i}^{N} b_{t_w} P_B}{\sigma^2}$. The system ergodic sum rate is written as

$$\varepsilon_S = \varepsilon_{SR} + \varepsilon_{ST}. \quad (17)$$

One can derive the expression of (17) on the basis of (16).

Remark 1: i) Both the outage and sum rate performances at IoDs are highly affected by P_b and L_a; ii) with an increasing SNR, both the metrics are saturated; iii) Due to channel correlation, the system performances also drop.

IV. Numerical Results

This section validate the analyses presented in the previous section through the Monte-Carlo simulations. The parameter settings are given in Table I. The average channel estimation errors and SIC imperfection factors are considered for the simulation as 0.05. d_{Ri}=d_{Ti}=$\{3, 6, 10, 12, 14, 16\}$ m, $(i \in 1, 2, \ldots, 6)$. The power allocation factors for NOMA are considered as $a_1 = 0.51$, $a_2 = 0.295$ and $b_1 = 0.1$, $b_2 = 0.095$. The amplification factor is $\alpha_1 = \alpha_2 = \cdots = \alpha_{L_a} = \alpha = 3$ dB and $\Upsilon_R^{th} = \Upsilon_T^{th}$. The vales of $d_x = d_y = \lambda/3$, $G_T = G_R = 20$ dB and $G = 1$ dB and the centralized location of transmitter, RIS are $(-50, 0, 10)$ and $(49, 0, -5)$, respectively. The dimension of RIS is considered as with $d_{\iota h}$=7.5 cm, $d_{\iota v}$=10 cm.

Fig. 2 shows the variation of the system outage performances of both RDs and TDs for both the near-field and far-field communication models with respect to P_B for $N_T = N_R = 2$ under the consideration of ICSI-ISIC for $L_a = 40$. Analytical results are well matched with the simulation results. As SINRs at IoDs grows with an increase of the transmission power of

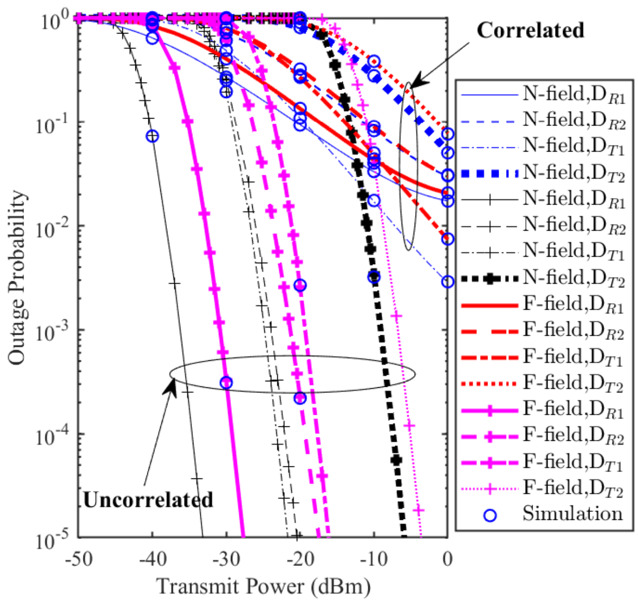

Fig. 2: System OP vs P_B comparisons between uncorrelated and correlated cases for both the near-field and far-field communication under ISIC-ICSI.

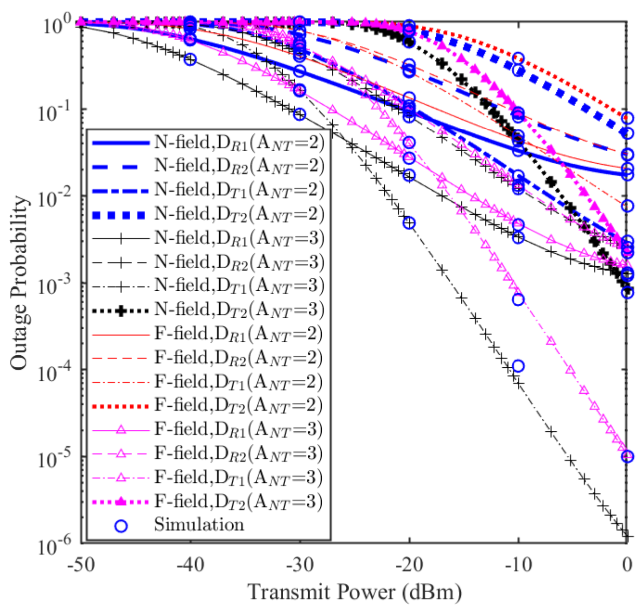

Fig. 3: System OP vs P_B comparisons between active and passive STAR-RIS under ISIC-ICSI.

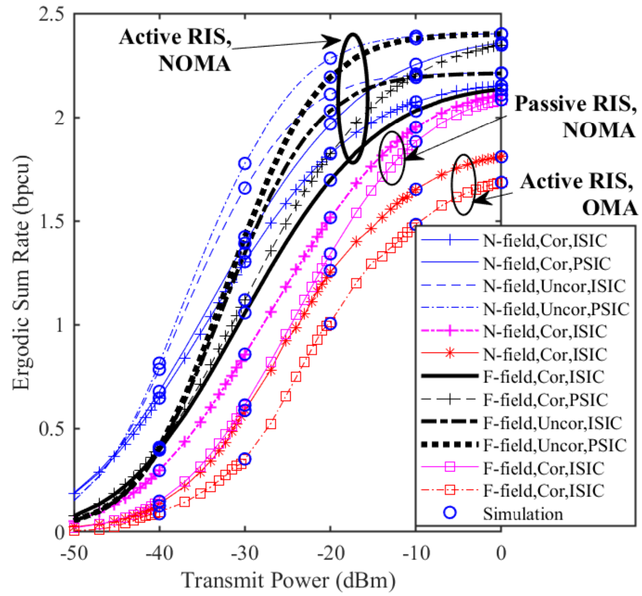

Fig. 4: Ergodic sum rate vs P_B comparisons between near-field and far-field at $L_a = 40$.

transmitter, consequently, OP of all the devices decrease at higher P_B. Due to channel correlation, the relative value of success probability of $\mathscr{P}(\Upsilon_{Ri\to Ti} \geq \Upsilon_R^{th})$ is lower at the given parameter settings and effectively, the OP of RDs are observed as poor compared to TDs.

The outage performance of the near-field adapted model is better than the far-field adapted model and the channel correlation leads to performance degradation as compared to uncorrelated channel model. Fig. 3 illustrates the performance improvement using active RIS over passive RIS. Fig. 4 presents the ergodic sum rate performance comparison between the near-field and far-field models for both PSIC-PCSI and ISIC-ICSI conditions. Initially, at low power, the performance of near-field communication is much better than far-field cases and thereafter the performances of both cases are almost the same at higher transmit power (10 dBm). Due to imperfections in SIC and channel estimation, the system performances are deteriorated. The results are compared with the performances of a similar system with the same parameter settings using passive STAR-RIS and the orthogonal multiple acces (OMA)-based active STAR-RIS for ISIC-ICSI condition. It is found that NOMA-based active and passive STAR-RIS performances for both near-field and far-field communication model are far better than OMA-based active STAR-RIS and we also observe that better performance is achieved through active STAR-RIS compared than passive STAR-RIS.

Fig. 5a and 5b depict the outage and ergodic sum rate variations at different distances between transmitter and center of RIS for ICSI-ISIC case at 30 dB SNR. As the centralized deployment is considered, therefore, RIS can move horizontally from the transmitter to IoDs. When RIS is closer to either transmitter or IoDs, the performance of the considered scheme is improved. The joint power radiation pattern (F_{gi}^{combine}, $\forall g \in R, T$) is non-linear in nature in case of near-field communication and it directly depends on the distance between d_{BR}. Therefore, as F_{gi}^{combine} changes, the outage and ergodic sum rate are also varying accordingly. If RIS is closer to either transmitter or IoDs, F_{gi}^{combine} changes in a such a way that both the performances are improved drastically. As all the components present within F_{gi}^{combine} are related to the cosine function, therefore, the outage and ergodic sum rates saturate after reaching a maximum value. However, in the case of far-field communication, the variation of F_{gi}^{combine} is linear in nature with the change of d_{BR}. Both outage and ergodic performances are found as poor for near-field communication

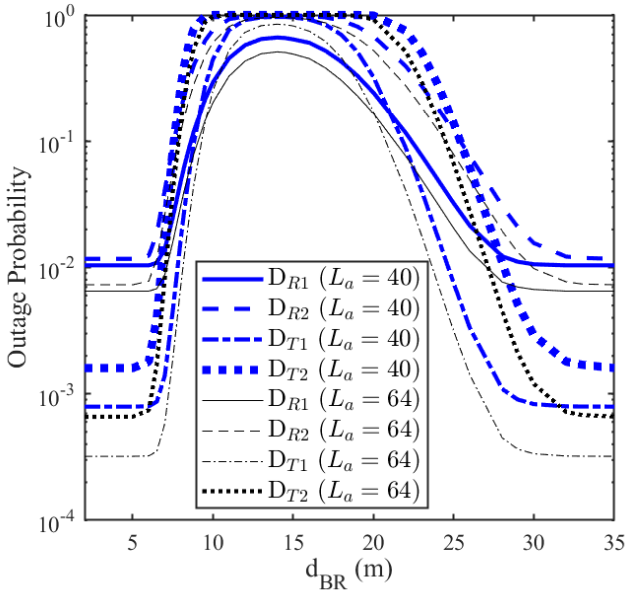

(a)

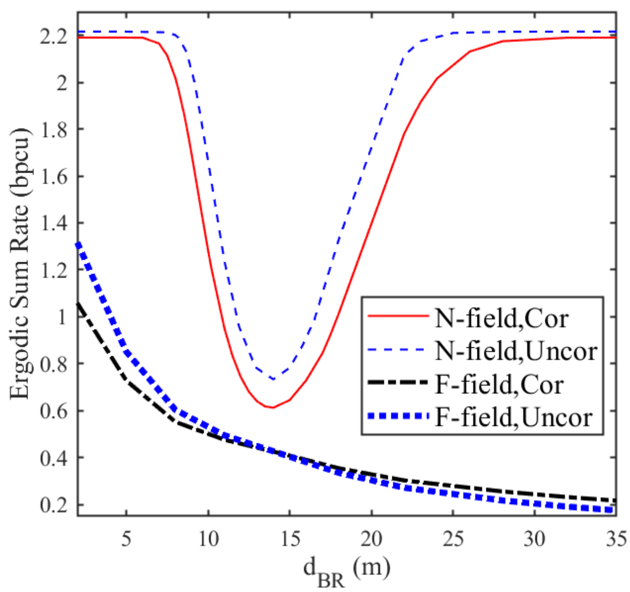

(b)

Fig. 5: (a) Correlated system OP vs d_{BR} plot for $L_a = 40$ and 64; (b) Ergodic sum rate vs d_{BR} plot at $L_a = 40$.

at intermediate distances between $10 - 20$ m. The outage performance is improved with the increasing value of L_a. The ergodic performance is observed as poor for far-field communication as compared to near-field communication.

V. Conclusions

This paper considered the effect of spatial channel correlation on the OP and ergodic sum rate performances of active STAR-RIS assisted near-field communication applying NOMA principle. Based on the different distances, the performance results were also shown through the perspective of both near-field and far-field communication. It was observed that the radiation pattern of near-field communication changes drastically with the variation of the distance between transmitter and active STAR-RIS. The consideration of multiple antennas at transmitter to analyze the performance of similar model is the future research direction. Through the results, it is shown that the performances of the system are degraded with ISIC and imperfect channel estimation.

References

[1] M. Di Renzo *et al.*, "Smart radio environments empowered by reconfigurable intelligent surfaces: how it works, state of research, and the road ahead," *IEEE J. Sel. Areas Commun.*, vol. 38, no. 11, pp. 2450–2525, 2020.

[2] Y. Liu *et al.*, "STAR: Simultaneous transmission and reflection for 360° coverage by intelligent surfaces," *IEEE Wireless Commun.*, vol. 28, no. 6, pp. 102–109, 2021.

[3] X. Mu, Y. Liu, L. Guo, J. Lin, and R. Schober, "Simultaneously transmitting and reflecting (STAR) RIS aided wireless communications," *IEEE Trans. Wireless Commun.*, vol. 21, no. 5, pp. 3083–3098, 2022.

[4] K. Zhi *et al.*, "Active RIS versus passive RIS: Which is superior with the same power budget?" *IEEE Commun. Lett.*, vol. 26, no. 5, pp. 1150–1154, 2022.

[5] F. Karim, S. K. Singh, K. Singh, S. Prakriya, and M. F. Flanagan, "On the performance of STAR-RIS-aided NOMA at finite blocklength," *IEEE Wireless Commun. Lett.*, vol. 12, no. 5, pp. 868–872, 2023.

[6] X. Yue, J. Xie, Y. Liu, Z. Han, R. Liu, and Z. Ding, "Simultaneously transmitting and reflecting reconfigurable intelligent surface assisted NOMA networks," *IEEE Trans. Wireless Commun.*, vol. 22, no. 1, pp. 189–204, 2023.

[7] S. Dhok and P. K. Sharma, "Rate-splitting multiple access with STAR RIS over spatially-correlated channels," *IEEE Trans. Commun.*, vol. 70, no. 10, pp. 6410–6424, 2022.

[8] T. Wang, M.-A. Badiu, G. Chen, and J. P. Coon, "Outage probability analysis of STAR-RIS assisted NOMA network with correlated channels," *IEEE Commun. Lett.*, vol. 26, no. 8, pp. 1774–1778, 2022.

[9] ——, "Performance analysis of IOS-assisted NOMA system with channel correlation and phase errors," *IEEE Trans. Veh. Technol.*, vol. 71, no. 11, pp. 11 861–11 875, 2022.

[10] Z. Ding, "Resolution of near-field beamforming and its impact on NOMA," *IEEE Wireless Commun. Lett.*, 2023.

[11] U. Singh *et al.*, "Performance analysis of the STAR-RIS-assisted downlink NOMA communication system with MRC," *IEEE Commun. Lett.*, vol. 27, no. 7, pp. 1739–1743, 2023.

[12] E. D. Carvalho, A. Ali, A. Amiri, M. Angjelichinoski, and R. W. Heath, "Non-stationarities in extra-large-scale massive MIMO," *IEEE Wireless Commun.*, vol. 27, no. 4, pp. 74–80, 2020.

[13] Y. Zhang *et al.*, "Reconfigurable intelligent surfaces with outdated channel state information: centralized vs. distributed deployments," *IEEE Trans. Commun.*, vol. 70, no. 4, pp. 2742–2756, 2022.

[14] Z. Zhang *et al.*, "Ergodic capacity of intelligent omni-surface-aided communication systems with phase quantization errors and outdated CSI," *IEEE Syst. J.*, vol. 17, no. 2, pp. 1889–1898, 2023.

[15] E. Björnson and L. Sanguinetti, "Rayleigh fading modeling and channel hardening for reconfigurable intelligent surfaces," *IEEE Wireless Commun. Lett.*, vol. 10, no. 4, pp. 830–834, 2021.

[16] T. Park, G. Lee, W. Saad, and M. Bennis, "Sum rate and reliability analysis for power-domain nonorthogonal multiple access (PD-NOMA)," *IEEE Internet Things J.*, vol. 8, no. 12, pp. 10 160–10 169, 2021.

[17] A. Papazafeiropoulos, H. Ge, P. Kourtessis, T. Ratnarajah, S. Chatzinotas, and S. Papavassiliou, "Two-timescale design for active STAR-RIS aided massive MIMO systems," *IEEE Trans. Veh. Technol.*, pp. 1–16, 2024.

[18] C. You and R. Zhang, "Wireless communication aided by intelligent reflecting surface: Active or passive?" *IEEE Wireless Commun. Lett.*, vol. 10, no. 12, pp. 2659–2663, 2021.

[19] C. Zhou, B. Lyu, S. Gong, and C. You, "Active STAR-RIS-assisted symbiotic radio communications under hardware impairments," *IEEE Commun. Lett.*, vol. 27, no. 10, pp. 2797–2801, 2023.

[20] J. W. Goodman, *Speckle phenomena in optics: theory and applications*. Roberts and Company Publishers, 2007.

[21] I. S. Gradshteyn and I. M. Ryzhik, *Table of integrals, series, and products*. Academic press, 2014.